TISSUE ENGINEERING

10.1126/sciadv.1500423

Platform technology for scalable assembly of instantaneously functional mosaic tissues

Boyang Zhang,[1,2]* Miles Montgomery,[1,2]* Locke Davenport-Huyer,[1,2] Anastasia Korolj,[1,2] Milica Radisic[1,2]†

Engineering mature tissues requires a guided assembly of cells into organized three-dimensional (3D) structures with multiple cell types. Guidance is usually achieved by microtopographical scaffold cues or by cell-gel compaction. The assembly of individual units into functional 3D tissues is often time-consuming, relying on cell ingrowth and matrix remodeling, whereas disassembly requires an invasive method that includes either matrix dissolution or mechanical cutting. We invented Tissue-Velcro, a bio-scaffold with a microfabricated hook and loop system. The assembly of Tissue-Velcro preserved the guided cell alignment realized by the topographical features in the 2D scaffold mesh and allowed for the instant establishment of coculture conditions by spatially defined stacking of cardiac cell layers or through endothelial cell coating. The assembled cardiac 3D tissue constructs were immediately functional as measured by their ability to contract in response to electrical field stimulation. Facile, on-demand tissue disassembly was demonstrated while preserving the structure, physical integrity, and beating function of individual layers.

INTRODUCTION

The aligned and integrated pseudolaminar syncytium of the myocardium is essential for electrical impulse propagation that translates into orchestrated cardiac fiber contraction and pumping of blood (*1*–*5*). The myocardium is also composed of multiple cell types, for example, cardiomyocytes (CMs), fibroblasts (FBs), and endothelial cells (ECs), precisely organized at the microscale level to achieve desired function (*6*). An ideal tissue culture strategy should therefore enable precise placement of different cell types, with the ability to control cell orientation in the *x*, *y*, and *z* direction. The tissue culture platform should also enable on-demand tissue assembly and disassembly with preservation of the structure and function of individual units so that independent treatment, follow-up analysis, or further coculture studies could be performed.

Recent technological advances in cardiac tissue engineering enable control of cell orientation in microfabricated anisotropic scaffolds (*7*–*10*), cell layering in hydrogels (*11*), and anisotropic cell orientation due to cell-gel compaction (*12*). Patterned scaffold meshes provided an anisotropic stiffness that mimicked the native myocardium (*8*, *9*), but the assembly of multiple tissue meshes into thick tissues was not possible (*13*, *14*). Bioprinting of cells in hydrogels was also used to study cell-cell and cell–extracellular matrix (ECM) interactions with high spatial and temporal control (*15*, *16*). Although bioprinting enables control of cellular position in three dimensions (3D) (*16*), it is difficult to remove selected individual tissue units from the bioprinted tissues, without tissue destruction. Furthermore, forming tissues with organized anisotropic structures requires robust tissue-level remodeling achieved by a high degree of hydrogel compaction by the seeded cells. This process is accompanied by a dramatic change in tissue size, making it difficult to predict final tissue shape, structure, and consequently function when starting from an initial hydrogel-based bioprinted or cast material. Tissue culture methods such as embedding cells in a hydrogel on a paper-based scaffold with random pore distribution have been implemented to rapidly cast thick tissues by stacking multiple scaffold units together (*17*, *18*), with the ability to perform the follow-up analysis by de-stacking the tissue layer. However, the combined ability to control cell orientation, mechanical anisotropy, and on-demand assembly/disassembly in a single system has not yet been achieved.

Therefore, we sought to develop a broadly applicable tissue culture system on the basis of a biodegradable and implantable material that enables (i) control of mechanical tissue anisotropy; (ii) coculture of different cell types with control of cell position; (iii) assembly in the *z* direction for construction of thick tissues; and (iv) on-demand, minimally invasive disassembly while preserving the structure and function of individual layers. These seemingly opposing goals were achieved by the development of Tissue-Velcro, a microfabricated biodegradable scaffold that provides structural cues to instruct cellular self-assembly into an organized *x*-*y* syncytium while enabling 3D tissue assembly and on-demand disassembly in *z* direction through a hook and loop mechanism similar to the conventional Velcro.

RESULTS

We envisioned designing living tissues that could be as easily and firmly assembled as two pieces of Velcro. Conventional Velcro (Fig. 1A) is composed of two sheets: one sheet is an array of hooks and the other is a sheet of fibers that form loops. When the two surfaces are brought into contact, the loops catch on the hooks and the layers remain attached until a sufficient pull-off force is applied. Not all hooks will attach to a loop, but when a sufficient number of hooks catch a loop over the contact area, significant adhesive force can be generated. Tissue-Velcro uses the same mechanical interlocking principle to lock two living tissue meshes together (Fig. 1A).

First, an accordion honeycomb mesh was fabricated through injection molding of a biodegradable elastomer, poly(octamethylene maleate (anhydride) citrate) (POMaC) (Fig. 1B). POMaC is a biodegradable (fig. S1) and ultraviolet (UV) photo-crosslinkable elastomer prepared through polycondensation reaction from the monomers (1,8 octandiol, citric acid, and maleic anhydride) under mild conditions (*19*). The bulk material exhibited a negligible drop in Young's modulus from days 1 to 7

[1]Department of Chemical Engineering and Applied Chemistry, University of Toronto, Toronto, Ontario M5S 3E5, Canada. [2]Institute of Biomaterials and Biomedical Engineering, University of Toronto, Toronto, Ontario M5S 3G9, Canada.
*These authors contributed equally to this work.
†Corresponding author. E-mail: m.radisic@utoronto.ca

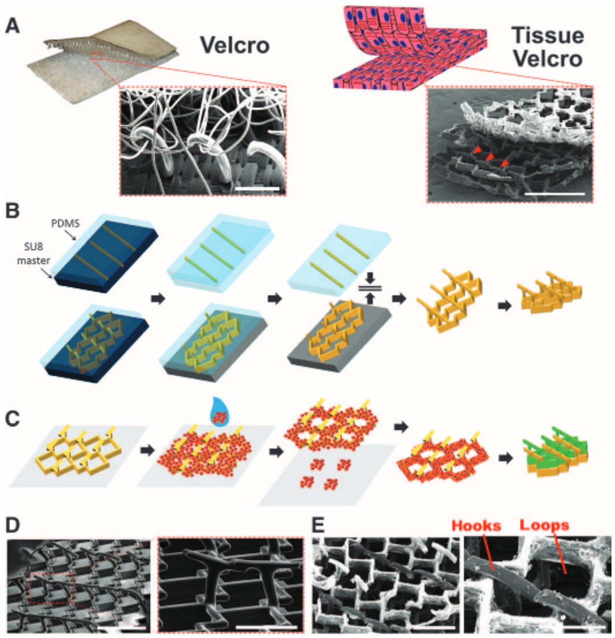

Fig. 1. Fabrication and physical characterization of the Tissue-Velcro platform. (**A**) The hooks and loops of the conventional Velcro system inspired the Tissue-Velcro design, based on a biocompatible and biodegradable polymer, POMaC. Red arrows indicate the built-in hooks. Scale bar, 1 mm. (**B**) Illustration of the fabrication process of the scaffold including a microinjection step followed by the stamping step. (**C**) Cell seeding process. A Matrigel-based cell suspension is allowed to gel on the scaffold, and when removed from the tissue culture, substrate holes are formed. After self-assembly, the compacted tissues can be handled and patterned. (**D**) SEM images revealed detailed scaffold architecture with the T-shaped hooks and an accordion mesh. Scale bar, 1 mm. Inset, high-magnification SEM of T-shaped hooks. Scale bar, 500 μm. (**E**) SEM image captures two scaffolds interlocking. The hooks from the bottom scaffold (dull gray) protrude above the struts of the top scaffold (white). Immediate detachment is prevented by these hooks of the bottom scaffolds catching on the struts of the top scaffold. Scale bar, 500 μm (left image); 300 μm (right image).

in culture medium in the presence of cells (fig. S1A). The bulk material mass loss was also negligible from days 1 to 14 (fig. S1B), whereas the initial mass loss could largely be attributed to porogen leaching during the rinsing step. The void spaces within the accordion honeycomb mesh function as the loops of the conventional Velcro system. Small T-shaped hooks were patterned by aligning and bonding a horizontal rectangular cap onto the posts on the base mesh (Fig. 1B). The cap was transferred with a poly(dimethylsiloxane) (PDMS) substrate, and the bonding was achieved by UV cross-linking (Fig. 1B). In the last fabrication step, the cap was incised to break the connection between the posts, establishing individually standing T-shaped hooks (Fig. 1B). Cell seeding was achieved by pipetting a cell suspension in Matrigel onto the scaffolds, allowing partial gelation (Fig. 1C), and then the scaffold was immediately lifted off the plastic tissue culture polystyrene substrate, allowing only the cells close to the scaffold struts to remain attached, thus producing small holes in the tissue (Fig. 1C). Overtime cells self-assembled around the scaffold structures (Fig. 1C). Subsequently, tissue patterning or stacking was performed with multiple tissues (Fig. 1C).

The microhooks of a single layer scaffold, which protrude through the void space of another scaffold mesh and anchor onto its struts, were imaged by scanning electron microscopy (SEM) (Fig. 1D). The SEM image of two tissues brought into contact shows the attachment mechanism whereby the hooks of the bottom scaffold protrude through the honeycomb mesh of the top scaffold and affix the two tissue meshes together (Fig. 1E). The maximum force recorded to pull off the scaffold was 6.2 ± 1.1 mN, or when divided by the area of the scaffold (2.5 × 5 mm), the pressure required was 0.5 ± 0.1 kPa. Typically 18 hooks (equivalent to 82% of total hooks) will successfully lock in place across the scaffolds when two 2.5 × 5–mm layers are brought into direct contact without offset. A 3D reconstruction from a confocal *z*-stack of an assembled two-layer scaffold construct shows the interlocking mechanism (movie S1). A representative plot of the pull-off test is shown in Fig. 2A (movie S2). The binding force between the two scaffolds is sufficiently strong to withstand manual manipulation such as stretching or compression (movie S3). The presence of cells on the scaffold or a short culture time between two layers (3 days) did not significantly affect the pull-off force (fig. S2). Thus, the hook and loop interlocking mechanism was primarily responsible for the mechanical stability of the assembled layers. The pull-off force was significantly higher when two scaffolds were overlaid by 100% (Fig. 2A, 6.2 ± 1.1 mN) in comparison to measurements in partially overlaid scaffolds (fig. S2B, 2.0 ± 0.9 mN, $P = 0.001$) as expected.

The accordion honeycomb pattern was chosen so that the scaffold exhibited spring-like elasticity, topographical cues for cell alignment, and anisotropic stiffness in the *xy* plane as described by Engelmayr *et al.* (*8*) (Fig. 2, B and C). In the linear region of the curve, the scaffold mesh displayed anisotropic mechanical properties with an anisotropy ratio of 1.3 ± 0.3. The apparent scaffold modulus was greater in the long axis (xD) direction (18.7 ± 2.5 kPa) compared to the short axis (yD) direction (14.4 ± 3.0 kPa, $n = 4$, $P = 0.067$). However, the scaffold strain expected from cell contraction is lower than the strain exhibited within the linear region (Fig. 2B). Within the physiological regime of scaffold strain of up to 15% as described (*8*), the scaffold mesh displayed anisotropic mechanical properties with an anisotropy ratio of 3.1 ± 1.6, and the apparent modulus was significantly greater in the xD (7.9 ± 1.8 kPa) compared to the *y* direction (2.6 ± 1.2 kPa, $n = 4$, $P = 0.002$). The feature heights of the scaffolds were measured using a profilometer, resulting in 53 ± 1–μm–tall hooks, positioned on top of 263 ± 5–μm–tall posts protruding off of the 132 ± 5–μm–thick mesh base for a combined total height of 448 ± 7 μm (Fig. 2, D and F).

The fibers of the mesh provided topographical cues to guide cellular assembly in the *xy* plane. Neonatal rat CMs were seeded onto the scaffolds with Matrigel, where the cells initially wrapped around the struts of the mesh and then remodeled the matrix by compacting and elongating around the struts over a period of 7 days (Fig. 3A and movie S4). After 4 to 6 days, the tissues displayed spontaneous contraction (movie S5). Cardiac tissue contraction was paced using an electrical stimulator (movie S6). As the tissue contracted, it compressed the scaffold in a spring-like fashion. Scaffold autofluorescence allowed for the deformation of the scaffold mesh under fluorescence microscopy to be tracked with image processing (movie S7). The degree of scaffold compression was characterized by tracking the decrease in the honeycomb area during contraction. A trend toward higher scaffold compression (percent area decrease at each beat) was recorded at day 6 compared

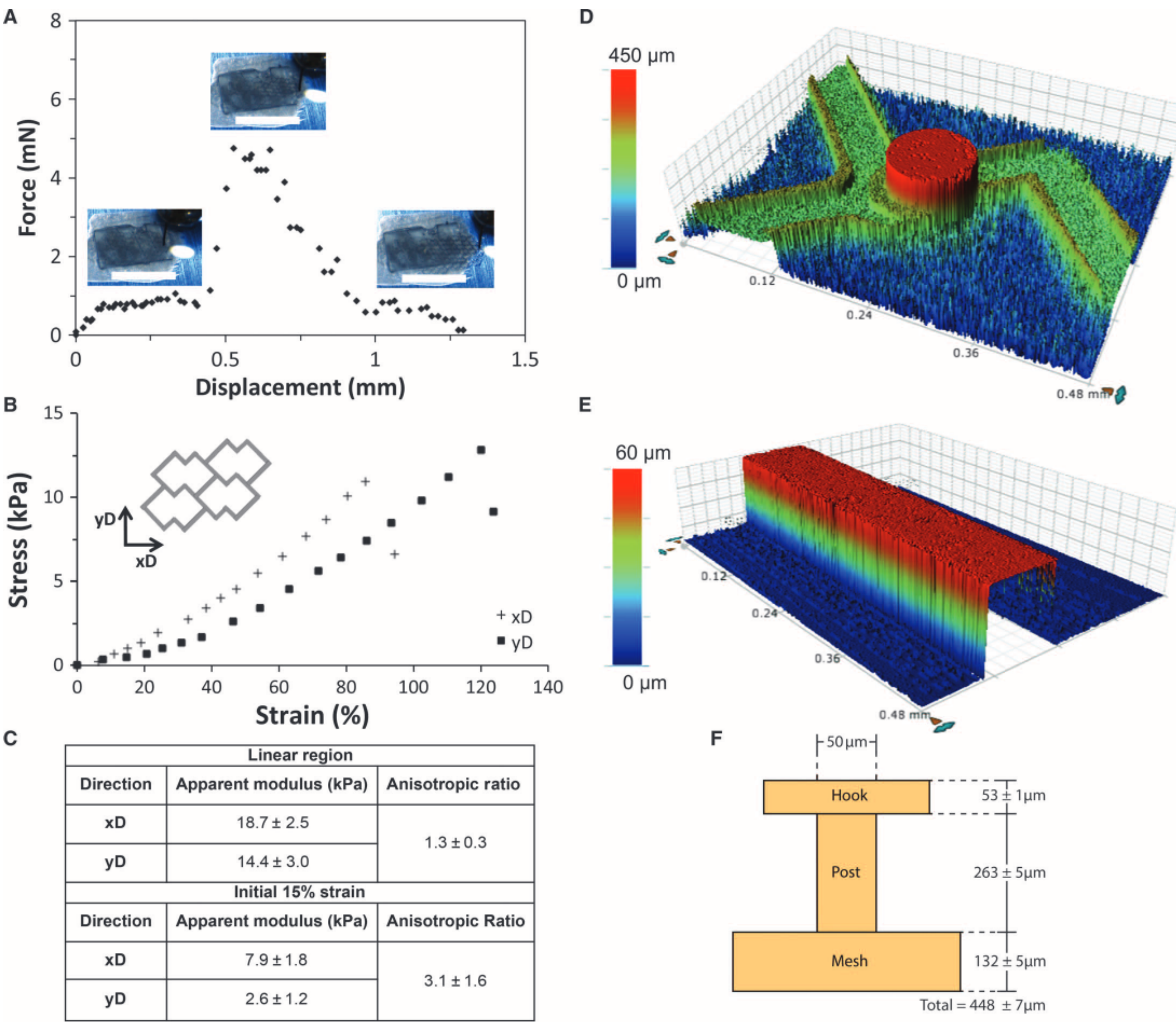

Linear region		
Direction	Apparent modulus (kPa)	Anisotropic ratio
xD	18.7 ± 2.5	1.3 ± 0.3
yD	14.4 ± 3.0	
Initial 15% strain		
Direction	Apparent modulus (kPa)	Anisotropic Ratio
xD	7.9 ± 1.8	3.1 ± 1.6
yD	2.6 ± 1.2	

Fig. 2. Mechanical properties of Tissue-Velcro. (**A**) Representative force curve from the mechanical pull-off test of the scaffold (n = 4). Inset scale bar, 5 mm. (**B**) Representative uniaxial tensile stress-strain plots of the scaffold in the x direction (xD) and y direction (yD) (n = 4). (**C**) Summary of the measured apparent modulus of the scaffold in the x direction (xD), y direction (yD), and the anisotropic ratio (xD/yD) (mean ± SD, n = 4). (**D** and **E**) Representative 3D renderings of profilometry data of the preassembled scaffold components. (D) Bottom mesh and post (n = 3); (E) top hook (n = 3). (**F**) Illustration of the cross-sectional view of an assembled scaffold labeled with measured heights (n = 3).

to day 4 (day 4: 0.87 ± 0.27%, day 6: 1.44 ± 0.07%, n = 3) (Fig. 3B). On day 8, the linear percent shortening was higher in the short-axis (yD) direction than in the long-axis (xD) direction (P = 0.038) (fig. S3), consistent with the lower modulus in the short-axis direction allowing for greater deformability (Fig. 2B). Immunofluorescence staining of the cytoskeletal actin filament F-actin and the contractile protein sarcomeric α-actinin and SEM revealed formation of a tissue layer with elongated CMs around the scaffold struts and visible cross-striations (Fig. 3, C and D, and fig. S4). Cardiac tissue was also able to exhibit a positive chronotropic response upon exposure to 300 nM epinephrine (fig. S5 and movie S11).

The compatibility of Tissue-Velcro with conventional coculture techniques was demonstrated by coating an additional layer of endothelial cells (ECs) on heart cells compacted around the mesh. This was achieved by adding an EC suspension to the tissue mesh for 24 hours and cultivating in the EC culture medium. CD31 immunofluorescence staining revealed a near confluent coating of ECs with cobblestone-like morphology around the tissue (Fig. 3E). A cross-sectional view of the tissue mesh coated with ECs costained with live cell tracker (green) and CD31 confirmed that the ECs covered the surface of the tissue and the heart cells occupied the inner core (Fig. 3F). The EC coating provided an additional dimension in the coculture assembly, a beneficial feature

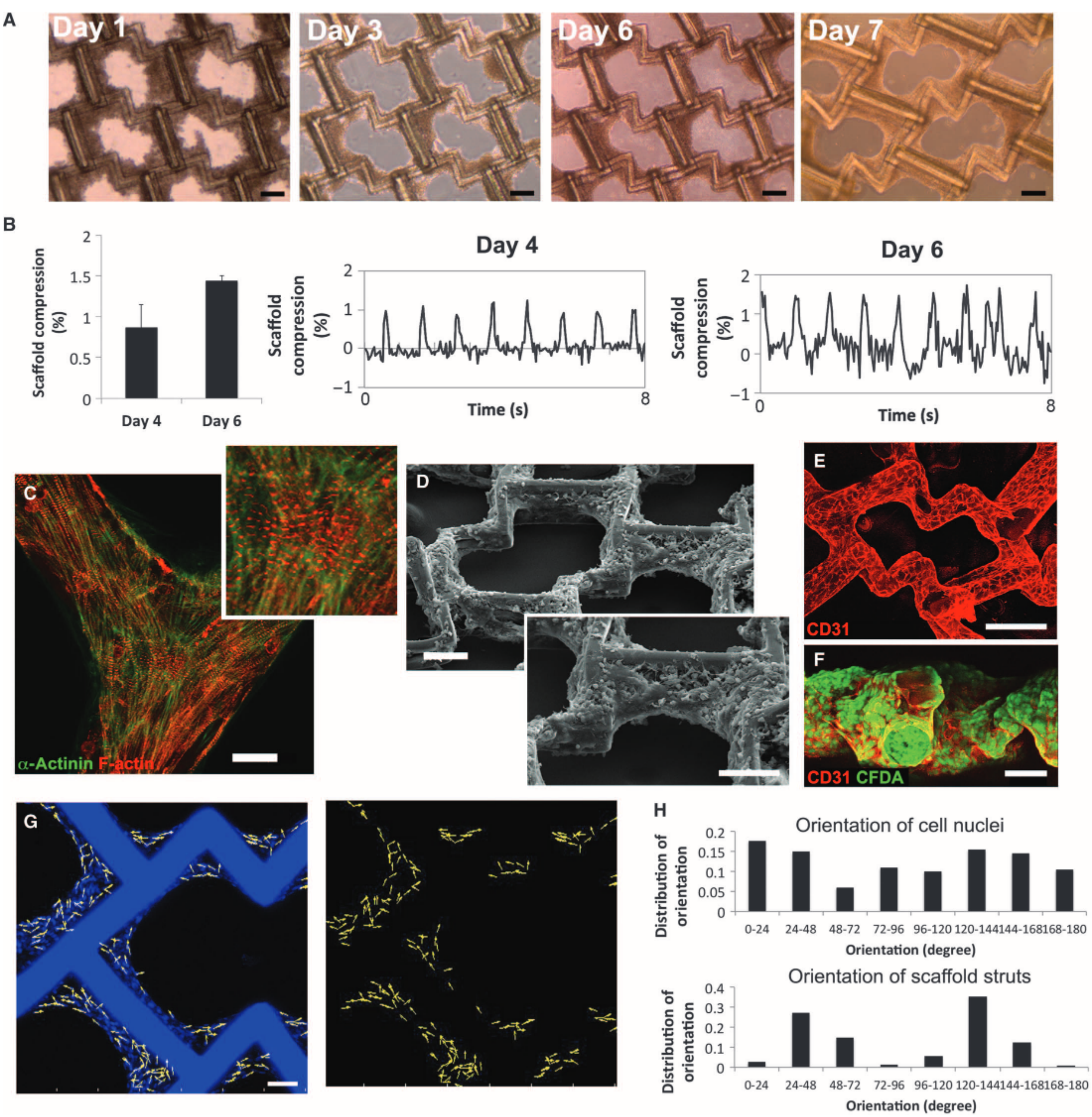

Fig. 3. Cardiac Tissue-Velcro characterization. (**A**) Cardiac cell assembly around a mesh over 7 days. Scale bar, 100 μm. (**B**) Area decrease (%) during 1-Hz paced contraction derived from scaffold deformation increased from day 4 to 6 (day 4: 0.9 ± 0.3%, day 6: 1.4 ± 0.07%, mean ± SD, n = 3). Representative plots of electrically paced (1-Hz) cardiac tissue contracting and compressing the scaffold on days 4 and 6 of culture (n = 3). (**C**) Immunostaining of cardiac Tissue-Velcro on day 7 with sarcomeric α-actinin (red) and F-actin (green) (n = 4). Scale bar, 30 μm. (**D**) SEM of a Tissue-Velcro showing tissue bundles (day 7); scale bar, 100 μm. Inset, high-magnification SEM of a segment of Tissue-Velcro; scale bar, 100 μm. (**E**) EC coating around 7-day-old cardiac tissue grew to confluence in 24 hours (CD31, red). Scale bar, 100 μm. (**F**) CFDA cell tracker (green)–labeled endothelial cells; scale bar, 50 μm. (**G**) Representative images of nuclear staining (DAPI, blue) overlaid with nuclear orientation vectors along the long nuclear axis (n = 3). Scale bar, 50 μm. (**H**) Normalized distribution of orientation angles for cell nuclei and scaffold struts, respectively (representative trace of n = 3).

if the entire tissue is to be perfused through its void spaces, where ECs can function as a barrier to shield the parenchymal cells from fluid shear stress. When culturing Tissue-Velcro in endothelial growth medium-2 (EGM-2) medium in an orbital flask bioreactor at 160 rpm with or without EC coating, EC coating helped to better maintain tissue structure (fig. S6). Scaffold guidance of cellular alignment was confirmed by comparing the normalized distribution of cell orientation measured from the main axis vector of the nuclei to the distribution of scaffold strut orientation (Fig. 3, G and H).

Individual tissues cultured in parallel were assembled simply by overlapping multiple tissues one on top of the other, allowing the hooks from one scaffold to grab onto the struts of the other scaffold (Fig. 4). This interlocking mechanism was achieved by a gentle compression of the two tissues together. Once affixed in place, each tissue could be separated by specifically peeling one off another; handling or manipulating the entire multilayer tissue did not disassemble the individual layers (movie S3). During assembly, different cell types cultured on different scaffold meshes were positioned strategically to stack the tissues in the *z* axis. To demonstrate this, we labeled rat cardiac FBs and rat CMs red and green, respectively, and affixed the layers together, instantaneously establishing coculture conditions (Fig. 4A). The two-layer stack had a thickness of 580 ± 5 μm, which was derived from the scaffold dimensions and based on the overlap configuration of two Tissue-Velcro scaffolds. Additionally, three cardiac tissue meshes labeled with two different fluorescent cell trackers were locked into one tissue construct (Fig. 4B and movie S8). The three-layer stack had a thickness of

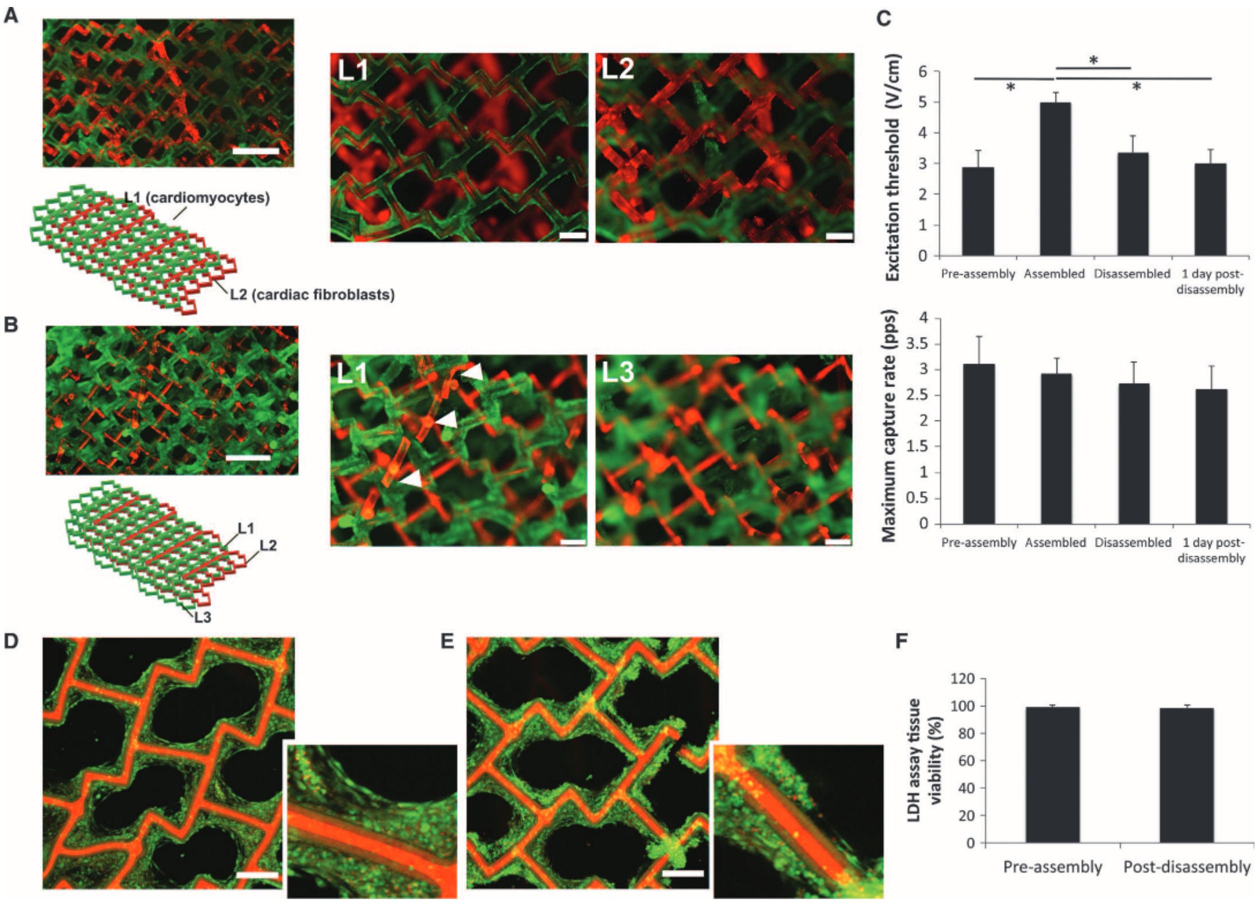

Fig. 4. Tissue function and viability upon assembly and disassembly. (**A**) Coculture conditions were instantaneously established in the *z* direction by assembling two layers of Tissue-Velcro (day 7): one consisting of cardiac FBs (red) and the second consisting of CMs (green). Scale bar, 800 μm. Tissue interlocking was visualized with high-magnification fluorescent images focusing on layer 1 (L1) and layer 2 (L2). Scale bar, 200 μm. (**B**) Assembly into a three-layer CM tissue construct. Scale bar, 800 μm. High-magnification fluorescent images focused on L1 and L3 confirm Tissue-Velcro interlocking. Scale bar, 200 μm. Arrowheads point to T-shaped microhooks protruding from the middle layer (L2) into the top layer (L1). (**C**) Electrical excitability parameters of the cardiac Tissue-Velcro (day 7) before assembly (mean ± SD, *n* = 8), after assembly (two-layer, mean ± SD, *n* = 4), after disassembly (mean ± SD, *n* = 8), and 1 day after disassembly (mean ± SD, *n* = 8). (**D** and **E**) Viability staining of CM Tissue-Velcro (day 4) (D) before (*n* = 3) and (E) after the tissue assembly/disassembly process (*n* = 4). Scale bar, 200 μm. CFDA, green; propidium iodide (PI), red. Scaffold struts exhibit autofluorescence in the red channel. (**F**) Quantification of tissue viability from LDH activity in tissue culture media collected before (mean ± SD, *n* = 8) and after the tissue assembly/disassembly process (mean ± SD, *n* = 4).

712 ± 7 μm. High-magnification images show the hooks from the red tissue mesh penetrated through and locked onto the struts of the green tissue mesh on top (Fig. 4B).

The electrical excitability properties of the cardiac tissues before assembly, after assembly (two-layer), after disassembly, and 1 day after disassembly were examined. Uniquely, the constructs contracted synchronously under electrical field stimulation, immediately after assembly (movie S9). We found that the excitation threshold (ET) increased slightly immediately after assembly and disassembly. However, the ET of the tissue decreased to its initial level 1 day after disassembly, likely due to tissue recovery (Fig. 4C). There were no changes in the maximum capture rate of the tissues throughout the process (Fig. 4C). Viability staining indicated the absence of appreciable tissue damage upon layer assembly and disassembly, with most of the cells staining positive for the viable dye carboxyfluorescein diacetate (CFDA; Fig. 4, D and E). Lactate dehydrogenase (LDH) assay quantified the tissue viability at greater than 98% and showed no significant difference in cardiac tissue viability before assembly and after the two-layer disassembly (Fig. 4F). Assembled tissues were cultivated for 3 days after assembly to demonstrate tissue integration between layers. SEM revealed that the hooks from the bottom tissue layer attaching onto the struts from the top tissue functioned as bridges allowing cell spreading and physical integration of the two layers (Fig. 5, A to C, and fig. S7). Three days after assembly, tissues demonstrated synchronized spontaneous contractions, indicating that the cell-cell connections between the layers have been established (movie S10).

To demonstrate the versatility of coculture patterning, we also assembled rat CM Tissue-Velcro horizontally in a checkerboard pattern (Fig. 5D). The length of the scaffold network was extended by coupling three scaffolds in an overlapping end-to-end fashion (Fig. 5E). Two cardiac tissues were also stacked at 45°, demonstrating the feasibility of varying the cell orientation throughout the tissue depth (in *z* direction) using this technology to ultimately mimic the gradual change in myofiber orientation in the ventricular wall of the heart (*20*) (Fig. 5F). The design of Tissue-Velcro is not limited to the accordion-mesh scaffold shape. Other designs with spring-like features (fig. S8) were also produced. These designs could be used in future studies to enhance anisotropic tissue alignment and percent shortening at contraction.

DISCUSSION

To accelerate the spatially organized tissue assembly and on-demand disassembly process, we introduce a new platform technology termed Tissue-Velcro. We previously demonstrated cellular alignment and compaction along a simple surgical suture (*21*). Here, we scaled the same concept to a more complex scaffold mesh. Cellular alignment

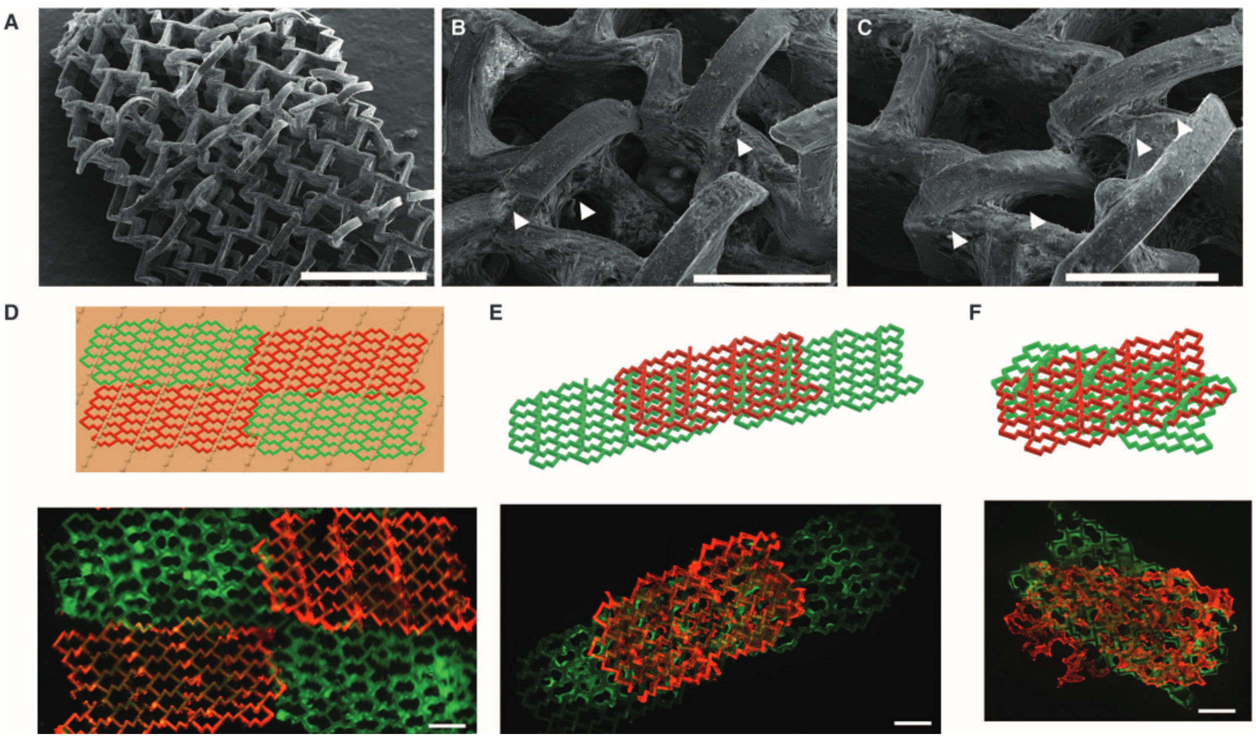

Fig. 5. Patterned mosaic tissue assembly. (**A** to **C**) SEM of two cardiac tissues (day 4) assembled together and then cultured for an additional 3 days (*n* = 4). (B and C) White arrows indicate locations where cells spread through a pathway created by the hook and loop configuration linking the two tissues together. Scale bars, 1 mm (A); 300 μm (B and C). (**D** and **E**) Tissues (day 7) composed of cardiac FBs were labeled either green or red and arranged into (D) a 2D pattern (scale bar, 800 μm) and (E) an offset 2D pattern to extend the length of the construct (scale bar, 800 μm). (**F**) Two cardiac tissues (day 7) were labeled either green or red and assembled together approximately at 45° angle. Scale bar, 800 μm.

is mainly attributed to the tension generated from the remodeling and alignment of the ECM against a template during the tissue formation process (*22*). Here, the template was the primary scaffold mesh. The scaffold mesh was made of a synthetic elastic biodegradable polymer that provided mechanical stability and allowed manual handling and assembly. The scaffold also provided topographical cues for cellular orientation in the desired direction, as well as the anisotropic mechanical stiffness designed to mimic the native myocardium. Furthermore, by adding T-shaped hooks onto the scaffold mesh, we created a Tissue-Velcro system allowing multiple cell types to be cultured individually and then assembled together vertically or horizontally to instantly establish a 3D mosaic coculture system that could be disassembled on demand.

While novel bioprinting techniques enable creation of tissues with a remarkable control over cell position, they do not allow for the release of cells or cell clusters without the destruction of the primary tissue structure. Additionally, reassembly of the primary tissue units into a new structure is not possible, and extensive time in culture is needed for cell orientation to be established in the gel-based systems (*12*, *23*). Elegant devices that pick, stack, and perfuse self-assembled cell structures have been developed, but the mechanical stability of these stacked structures was achieved only after ~48 hours when the cell-matrix remodeling resulted in the fusion of individual parts (*24*). Stackable polymeric scaffolds for scalable heart tissue engineering have been reported; however, they are created by sequentially stacking and solvent-bonding individual polymer layers followed by neonatal rat heart cell seeding and perfusion culture (*25*). Thus, the layers in the stacked device are not individually addressable and cannot be disassembled after the tissue is formed.

We adopted the general strategy of bottom-up tissue engineering using microfabrication techniques to generate a miniaturized scaffold that can guide tissue remodeling followed by the assembly, with immediate functionality, into 3D cardiac tissue while preserving the original tissue structure and topography. Injection molding of photo-crosslinkable POMaC enabled the fabrication of a variety of scaffold structures. POMaC was selected because of its biocompatibility as an implantable biomaterial, biodegradability, and the potential to tune scaffold mechanical properties and processability in a wide range through the dual (temperature and UV) cross-linking mechanism (*19*). The Young's modulus of the base material was initially 552 kPa, then 510 kPa upon 1 week in the presence of the cells and culture medium (fig. S1). The Young's modulus of the adult human myocardium was reported to to be in the range of 200 to 500 kPa in the contracted state (*26*–*29*); thus, the polymer has physiologically relevant bulk elasticity. Our novel microfabrication method allowed additional features to be patterned onto the 2D mesh to form intricate 3D structures, such as microhooks. The individual tissue meshes were assembled into functional 3D tissue with the use of a hook and loop mechanism, thus creating 3D functional tissues, for example, a cardiac tissue capable of macroscopic contractions. Although other cardiac tissue engineering techniques also provide tissues with a small percent of shortening at each beat (*13*), it is necessary to improve this functional parameter in order for the patches to become useful in the context of heart repair. If nonmyocyte layers such as FBs or EC-tissue layers were used for 3D assembly, the coculture effect would take more time to become apparent because these cells are not capable of contractile activity. In other coculture methods that may include spatially defined cell positioning using hydrogels, as in bioprinting or soft lithography, CMs are rounded and do not form interconnected syncytium immediately after seeding. Thus, they are not capable of immediate contraction upon tissue fabrication, and several days may be required for the cells to attach to the matrix, elongate, and connect so that they can exhibit a synchronous contractile function.

This tissue engineering strategy could also eliminate the need for a complicated perfusion bioreactor for in vitro culture of thick tissues. Each thin tissue mesh can be cultured separately without oxygen deficiencies and then assembled into a thick tissue construct before implantation. After assembly, the mass transfer of oxygen and nutrients could also be enhanced by the presence of void spaces within the tissue construct. An additional advantage of the Tissue-Velcro 3D scale-up is that each layer is prefabricated and fully functional with a completed cell/gel remodeling process. This prevents a large-scale size change and delay in functionality that is usually observed with remodeling of 3D cell/hydrogel systems.

Coculture is a tool used by cell biologists and tissue engineers for improving vascularization and cell survival by implementation of supporting signals that recapitulate an in vivo niche (*6*, *14*). Because a cell suspension can easily penetrate through the mesh structure, this allows ECs to coat around the tissue fibers on the Tissue-Velcro scaffold mesh. ECs were previously demonstrated to support CM survival and viability in coculture (*30*, *31*). In the native myocardium, ECs are organized in dense, branching tubular vascular structures with parallel capillaries in intimate contact with CM bundles, such that each CM is positioned no more than 20 μm from the capillary (*32*, *33*). The described Tissue-Velcro geometry does not capture the complexity of the native EC arrangement in a tubular branching vasculature, but it provides two important aspects of the native EC-CM configuration. First, EC coating in direct coculture provides protection from shear because coated CMs are not directly exposed to the flowing media. Second, ECs and CMs are in close physical proximity on Tissue-Velcro, potentially enabling paracrine signaling between the two cell types, which usually decay rapidly as a function of spacing (*34*, *35*). The ability to coat the tissue with ECs can be beneficial when implanting the tissue. For example, the presence of tissue modules coated with ECs has been shown to enhance in vivo anastomosis and tissue survival (*36*). Modular tissue coculture systems consisting of ECs and bone marrow–derived mesenchymal stem cells supported the survival and stable chimeric blood vessel anastomosis of ECs in vivo (*37*). Infiltration of cells from the host and implant integration could also be enhanced because of the macroporous tissue structure (*38*). Implanted cardiac cell sheets cocultured with ECs were observed to have improved anastomosis and neovascularization (*39*).

The described platform technology also allows coculture of multiple cell types in different tissue layers (such as CMs and cardiac FBs). The importance of FBs in cardiac tissue engineering has been well documented (*40*, *41*). For example, a nonmyocyte preculture to support CMs resulted in improved cardiac organoid structure and function (*35*). Enhanced connexin-43 levels were achieved with the release of vascular endothelial growth factor secreted by precultured FBs (*31*). The Tissue-Velcro platform is compatible with sequential assembly of different cell types (for example, cardiac FBs followed by CMs) in a defined temporal sequence, thus potentially enabling preconditioning of the environment for the target cell type survival and optimized function. In the native myocardium, FBs are interspersed between CM (*4*). Alternating layers of CMs and FBs are used here to show the versatility of the technique and provide paracrine signaling. Stacking several CM layers has more physiological relevance than alternating CM/FB layers in the scaled-up tissue.

POMaC material is well suited for cardiac tissue engineering because it is an elastomer that can be dynamically stretched and return to its original shape over cyclic loading; the honeycomb design further enhanced this property. The honeycomb design was previously investigated using poly(glycerol sebacate) and excimer laser microablation, a technique that cannot generate complex hook-shaped structures in the *z* axis (*8*). The use of 3D stamping together with injection molding was critical for the formation of T-shaped hooks here. Furthermore, recreating a graft that will integrate with the host myocardium and provide maximal therapeutic benefit requires structural reinforcement (*42*, *43*) and appropriate anisotropy (*44*, *45*) from the grafts. The developed scaffold meshes have mechanical properties (Fig. 2B) similar to the native rat neonatal myocardium (4.0 to 11.4 kPa) (*46*) but still allowing for deformation and mechanical transfer of the CM contraction. Each layer of the current Tissue-Velcro design is thick compared to the individual laminar layers of the myocardium. Using soft lithography, we could create polymer layers as thin as 10 to 20 μm; however, the mechanical stability of the overall structure would decrease, necessitating the use of polymer composition with a higher Young`s modulus and denser spacing of the scaffold struts.

The stable polymeric structure makes Tissue-Velcro less susceptible to damage due to physical handling during delivery. The meshes were easily handled with forceps and assembled into a desired pattern or arrangement. Compared to techniques such as cell-sheet technology (*47*) or collagen-based tissue mesh (*23*), Tissue-Velcro maintained its own structure without external substrate support, and it was flexible enough to regain its shape after deformation.

Tissue-Velcro is a platform technology based on a biocompatible, implantable, and biodegradable polymer, which can easily be transferred, in future studies, to cell coculture in multiple settings (for example, for skin or liver tissue engineering). The ability to dynamically control both spatial and temporal culture parameters enables the potential use of this technology in cell differentiation, for example, timed application of growth factors and selective, timed cell-cell contact. Alternatively, individual cell layers could be separately treated with different survival factors before assembly of the tissue for implantation to maximize its ability to survive in inflammatory or hypoxic environments. The ability to disassemble the tissues on-demand may provide a tool for spatially defined follow-up studies, for example, to determine how cell viability, metabolism, or gene expression varies as a function of thickness in different culture or implantation conditions. These individual layers from different tissue depths and various cultivation conditions could then be strategically recombined to study the possibility that cells retain memory of their previous environment, with a view of optimizing cell survival and differentiation protocols for in vitro and in vivo studies.

MATERIALS AND METHODS

POMaC prepolymer synthesis

The Tissue-Velcro scaffold was made out of an elastic, biodegradable, dual cross-linkable (heat and UV) elastomer (POMaC) as synthesized previously (*19*). Briefly, 1,8-octanediol, maleic anhydride, and citric acid were added to a 250-ml triple-neck flask at a molar ratio of 5:1:4, respectively. The reaction vessel was heated to 160°C and stirred until a clear solution was formed before subsequently decreasing the temperature to 140°C for 3 hours under nitrogen purge. Then, POMaC prepolymer was dissolved in ethanol and purified by drop precipitation into deionized water followed by 3 days of lyophilization. The purified POMaC prepolymer solution was then mixed with poly(ethylene glycol) dimethyl ether (PEGDM; M_w ~500, Sigma) at 60 and 5 wt % UV initiator (2-hydroxy-1-[4(hydroxyethoxy)phenyl]-2-methyl-1 propanone, Irgacure 2959). Poly(ethylene glycol) was used as a porogen to reduce the viscosity of the prepolymer solution during injection into the mold. The porogen was leached out in phosphate-buffered saline (PBS) after scaffold fabrication.

POMaC degradation

Pre-POMaC strips (1.5 mm × 0.5 mm × 10 mm) were exposed to a UV (365 nm) dose of 8100 mJ/cm^2. The strips were weighted in sets of 10 to determine initial mass. They were then soaked in PBS for 2 hours, followed by 70% ethanol overnight, and then washed two times in PBS. The strips were then placed into Transwell inserts (one strip per well) of a 24-well plate, with rat CMs seeded at the bottom and cultivated in the CM culture medium. Strips were collected at days 1 and 14, washed twice in deionized distilled water, and lyophilized for 3 days. Final mass was recorded and reported at each time point as percentage of mass lost compared to the immediately fabricated scaffold (day 0).

Scaffold fabrication

The device was fabricated using standard SU-8 photolithography techniques as previously described (*48*). Briefly, SU-8 photoresist was spin-coated on silicon wafers according to the manufacturer's guidelines. SU-8 photoresist was exposed to 365-nm UV, using a mask aligner (Q2001, Quintel Co.) through transparency masks with features of desired shape. The multilayered device required proper alignment between the features on the first and second layers before exposure. The nominal width of the mesh and the hooks was 50 and 100 μm, respectively, whereas the height of the bottom layer (mesh), the middle layer (post), and the top layer (hooks) was 132 ± 5 μm, 263 ± 5 μm, and 53 ± 1 μm, respectively. Finally, the master mold was submersed in SU-8 developer solution until all the unexposed photoresist was dissolved from the surface. A negative of the mold was made by pouring PDMS elastomer with a curing agent (17.5:1 ratio) and curing at room temperature for 3 days (Fig. 1B). The PDMS molds were then capped with either a glass slide or a flat sheet of PDMS to form a closed network of channels (Fig. 1B). The POMaC prepolymer/porogen/UV initiator mixture was then slowly injected through the mold at the inlet and left overnight to allow trapped air bubbles to dissipate. The PDMS molds were exposed to 2400 mJ/cm^2 (the exact UV exposure energy was fine-tuned for each batch of prepolymer solution) followed by peeling PDMS molds from either the glass or the PDMS cap. A PDMS mold and a glass slide with the scaffold were aligned and pressed together and exposed to 2400 mJ/cm^2 to covalently bond the two layers together (Fig. 1B). The connections between each T-shaped hook on the scaffold were then cleaved with Vannas spring scissors (Fine Science Tools) (Fig. 1B). The T scaffold was then removed from the substrates and placed in PBS (Fig. 1B). Individually cultured tissues were then assembled with fine tweezers by manual manipulation at the specified time point.

Scaffold structure characterization

SEM was used to assess scaffold and tissue structure, using a Hitachi SEM S-3400 in secondary electron mode at the Microscopy Imaging Laboratory, Faculty of Medicine, University of Toronto. Before imaging, the tissues were fixed in a 1% glutaraldehyde/4% paraformaldehyde (PFA) mix overnight at 4°C, washed in PBS, and dehydrated in sequential washes of 50, 70, 95, and 100% ethanol, followed by critical point drying. Optical profilometry (Bruker Contour GT-K, 10× parfocal objective) was used to assess the height of the scaffold features.

Pull-off force measurement

The pull-off force of the scaffolds was measured in PBS with Myograph (Kent Scientific). One scaffold was first glued to the bottom of a petri dish or pinned down with two micropins to a PDMS base in a petri dish. If the scaffold was glued to the bottom of the petri dish, the second scaffold placed on the top overlaid the bottom scaffold by 100%. In the case of scaffolds cultivated with cells, glue could not be applied, and they were pinned down to the PDMS-coated petri dish. Then, the upper scaffold of tissue was applied in the partly offset configuration in order not to interfere with the pin. A microneedle connected to the 2-g force transducer was hooked onto the outer right strut of the top scaffold, and it was pulled rightward with a micromanipulator until the top scaffold layer was completely released. The force generated during the process was recorded, and the maximum peak force before release was the pull-off force. The last data point collected after complete scaffold release was used as the baseline for force measurement. The nominal area of the scaffold (2.5 × 5 mm) was used in calculation.

Mechanical characterization

The mechanical properties of the scaffold were measured in PBS with a Myograph (Kent Scientific) in the long- and short-edge direction. The slope of the uniaxial tensile stress-strain curve from the first 15% strain was used to approximate the physiological regime, and the linear portion was used to calculate the effective elasticity as described (*8*, *49*–*51*). To determine the linear region, the entire data set was fitted using a least-squares regression followed by repeatedly dropping the lowest strain data point until the maximum R^2 value was achieved. The anisotropy ratio was determined by dividing the effective elasticity in the long-edge direction with the effective elasticity in the short-edge direction. The initial scaffold length and width were measured with a caliper for stress calculations.

Tensile tests were also conducted on samples of cross-linked POMaC strips, prepared in the mold with dimensions of 1.5 mm × 0.5 mm × 10 mm, to determine the mechanical properties of the bulk material over time. Strips were prepared and treated as described in POMaC degradation. Strips were collected and tested 1 and 7 days after exposure to cells and culture medium. Tensile testing was performed by pulling POMaC strips, submersed in PBS, along the length of the sample with a Myograph (Kent Scientific). Stress and strain relationships were plotted, and the Young's modulus was taken from the slope of the linear portion of the curve.

Neonatal rat heart cell isolation

Neonatal rat heart tissue was digested as described previously (*13*). Briefly, neonatal (1- to 2-day-old) Sprague-Dawley rats were euthanized, and the hearts were excised and placed in ice-cold Ca^{2+}- and Mg^{2+}-free Hanks' balanced salt solution (HBSS) (Gibco). Before quartering the heart, the aortic and vena cava structures were removed. Heart sections were rinsed twice in ice-cold HBSS and digested in a 0.06% (w/v) solution of trypsin (Sigma) in HBSS overnight at 4°C. Collagenase II (Worthington, 220 U/ml) in HBSS was used to further digest the heart tissue at 37°C in a series of five 4- to 8-min digestions. After the collagenase digestion, cells were preplated for 40 min. The nonadherent cells were used as the enriched CM population. The purified cardiac FB population was obtained from the adherent cells. Cardiac FBs were cultured and passaged once before use.

Cell seeding and culture

Cell-hydrogel preparation was carried out as similarly described by Nunes *et al.* (*21*). Briefly, a desired number of freshly isolated CMs or cardiac FBs were first pelleted and suspended in a liquid Matrigel solution at a ratio of 1 million cells to 1 μl of Matrigel solution. Typically, a 20-μl cell/Matrigel mixture was made at a time. Before cell seeding, the scaffolds were coated in a 0.2 wt % gelatin solution in PBS at 37°C for 4 hours to facilitate cell attachment. Two microliters of cell suspension was pipetted onto the scaffold to cover the scaffold with cells in a six-well cell culture plate (Fig. 1C). Excessive gel was removed until only a thin layer of gel/cell suspension covered the scaffold. The plate was then placed in an incubator for 4 to 6 min to allow the Matrigel mixture to partially gel. Prewarmed culture medium was then added, and a cell scraper was used to gently scrape the scaffold off the bottom of the plate. After the scaffold (initially fully covered with cells) was lifted, holes were then formed at the center of each honeycomb of the scaffold mesh because of the lack of structural support (Fig. 1C). Cells located near the scaffold struts remained on the scaffold. The medium was changed every 48 hours. The tissue constructs were cultured for 1 week before assembling and imaging (Fig. 1C). Rat CMs and cardiac FBs were cultured in Dulbecco's modified Eagle's medium (Gibco) containing glucose (4.5 g/liter), 10% (v/v) fetal bovine serum (FBS; Gibco), 1% (v/v) Hepes (100 U/ml; Gibco), and 1% (v/v) penicillin-streptomycin (100 mg/ml; Gibco).

Endothelial cell coating

Human umbilical vein endothelial cells (HUVECs) were purchased from Lonza and cultured with EGM-2 (Lonza) according to the manufacturer's instructions. Passage 3 to 5 HUVECs were used for all experiments. To coat the tissue meshes with endothelial cells, the tissues were immersed in 200 μl of endothelial cell suspension with 50 million cells/ml for 2 hours to allow endothelial cell attachment. The cell suspension was gently disturbed once every 30 min. Two milliliters of culture medium was then added, and tissue was incubated overnight to allow endothelial cell proliferation. EGM-2 was used for coculture conditions with rat CMs and HUVECs. Cocultured constructs were cultured for 2 days to allow for a confluent EC layer to form before imaging. Tissue-Velcro scaffolds coated with ECs or without ECs were also cultured in 25 ml of EGM-2 medium in 125-ml shaker flasks orbiting at 160 rpm, for an additional 3 days before imaging.

Functional characterization of cardiac tissues

Assessment of the contractile behavior of the cardiac sheets was measured using an S48 Grass Stimulator (Grass Technologies/AstroMed Inc.) as previously described (*13*, *35*). At day 7 after seeding, cardiac sheets were placed into stimulation chambers and stimulated with a biphasic square 2-ms pulse duration at 1 Hz. The ET (in volts per centimeter) was determined by increasing the output from 0 V at 0.1-V increments until synchronous cardiac sheet contraction was observed in unison with the stimulator output. The maximum capture rate (in hertz) was determined by setting the output voltage to double the ET and increasing the frequency of stimulation in 0.1-pps (pulse per second) increments until the cardiac sheet beating could not keep pace with the stimulator output. Video analysis as shown in movie S7 was performed in ImageJ (version 1.47v) first by thresholding the video followed by outlining the scaffold to acquire a single tracer outline of the struts of the scaffold mesh. Using this outline, the change in the area of the honeycomb mesh was tracked overtime (movie S6). The degree of scaffold deformation was derived from the decrease in the honeycomb size due to tissue contraction. The shortening of the long and short axis was measured using image analysis to detect the percentage shortening. Cell orientation on the tissues was characterized with ImageJ from the confocal images of the tissues stained with 4′,6-diamidino-2-phenylindole (DAPI). Each section of the confocal *z*-stack was processed separately. The cell nuclei were selected from the images with thresholding and then turned into binary images. Nuclei that appeared merged together or out of focus were eliminated. The orientation of each selected nucleus was then plotted in MATLAB with the Quiver function. Orientation of the scaffold struts was quantified using an ImageJ plug-in, OrientationJ (*52*), from the same confocal *z*-stack images. The Erode function in ImageJ was used to filter out the small cell nuclei and leave out only the scaffold struts. The images were then processed and plotted with OrientationJ. To stimulate cardiac tissues with drugs, epinephrine was first dissolved in HCl (12.1 N) and was then diluted to 0.3 μM in CM culture medium. Drug solution was applied to spontaneously beating tissue, and the response of the tissue was recorded.

Immunofluorescence staining

Immunofluorescence staining was performed to assess the morphology of the cultivated tissues. The tissues were first fixed in 4% (w/v) paraformaldehyde in PBS for 15 min at room temperature. Then, the cells were permeated and blocked in 5% FBS and 0.25% Triton X-100 in PBS for 1 hour. Next, the tissues were incubated in primary antibody against sarcomeric α-actinin (mouse, 1:200, Abcam, ab9465), overnight at 4°C, followed by incubation with a secondary antibody, Alexa 488–conjugated anti-mouse immunoglobulin G (IgG) (1:200, Life Technologies, A21202) and a phalloidin 66–conjugated anti–F-actin (1:300, Life Technologies, A22285). Tissues were then washed and imaged with confocal microscopy (Olympus FV5-PSU confocal with IX70 microscope). To visualize the endothelialized coating, the tissues were fixed in 4% PFA and blocked in 5% FBS for 1 hour. Then, the scaffolds were incubated in primary antibody, CD31 (mouse, 1:200 dilution, MAB2148), followed by incubation with secondary antibody, Alexa 647–conjugated anti-mouse IgG (1:200 dilution, Sigma). To visualize the tissue in the coculture experiments, before assembly, each tissue was incubated in either CFDA–succinimidyl ester (CFDA-SE; 1:1000, Life Technologies, C1157) or CellTracker Red (CMPTX, 5 μM, Life Technologies, C34552) in PBS at 37°C for 30 min. Assembled tissue constructs were imaged immediately after assembly. DAPI was used to visualize cell nuclei.

Tissue viability and LDH assay

Tissue viability was visualized with CFDA-SE (1:1000, Life Technologies, C1157) and PI (Life Technologies, P3566) in PBS as shown previously (*53*). Cell death analysis was performed on culture media collected from tissues before assembly and after disassembly using an LDH Cytotoxicity Assay Kit (Cayman Chemical Company) as per the manufacturer's instructions. Tissues were also lysed with 0.1% Triton X-100 to release all the LDH from the cells in a tissue construct as a baseline for 0% viability. The percentage of dead cells was determined by dividing the LDH measured in the media by the total LDH released upon cell lysis. To obtain the percentage of viable cells plotted in the graph, the percentage of dead cells was subtracted from 100%.

Statistical analysis

Error bars in figures represent SD. Statistical analysis was performed using SigmaPlot 12. Normality and equality of variance for the data were tested, and an appropriate statistical test was used. Statistical analysis in Figs. 2C and 3B and figs. S1B, S3A, and S6 (C and D) was done using Student's *t* test. Statistical analysis in Fig. 4C and fig. S2 (B and C) was performed with one-way analysis of variance followed by the Tukey-Kramer test. For Fig. 4F and fig. S1, the Mann-Whitney rank sum test was used. A P value of <0.05 was considered significant. A minimum of three samples were used per data point, as indicated in the figure captions.

SUPPLEMENTARY MATERIALS

Supplementary material for this article is available at http://advances.sciencemag.org/cgi/content/full/1/7/e1500423/DC1

Fig. S1. Base material physical properties under cell culture conditions.
Fig. S2. Hook and loop interlocking mechanism is a dominant factor governing the mechanical stability of the assembled two-layer structures.
Fig. S3. Cardiac tissue contractility.
Fig. S4. Immunostaining of cardiac Tissue-Velcro on day 7 for sarcomeric α-actinin (red) and F-actin (green) at various locations of the tissues.
Fig. S5. Drug response.
Fig. S6. Coculture of cardiac and endothelial cells.
Fig. S7. Scanning electron micrograph of the assembled two-layer cardiac tissue cultivated for 3 days.
Fig. S8. Scanning electron micrograph of an additional Tissue-Velcro design with spring-like structures that could potentially be used to enhance scaffold anisotropic mechanical properties and tissue anisotropic contraction.
Movie S1. The 3D confocal reconstruction of two interlocked scaffolds shows the hooks from the scaffold on the lower layer catching on the struts of the scaffold on the upper layer.
Movie S2. Recording of a mechanical pull-off test to measure the force required to detach interlocked scaffolds.
Movie S3. Two interlocked cardiac tissue layers were manipulated with tweezers, demonstrating that assembled multilayer tissue constructs can be handled and manipulated.
Movie S4. Time lapse of seeded CMs remodeling and compacting over a 3-day period on a single layer scaffold mesh (no hooks).
Movie S5. Contraction of cardiac tissue mesh after tissue remodeling, day 4.
Movie S6. Electrical field stimulation applied to a single scaffold mesh (no hooks) seeded with CMs, after 7 days in culture.
Movie S7. Autofluorescent scaffold contraction recorded and processed to measure fractional shortening.
Movie S8. Vertical scan of a three-layer Tissue-Velcro.
Movie S9. Electrically paced cardiac tissues contracting before assembly, after assembly, after disassembly, and 1 day after disassembly.
Movie S10. Spontaneous contraction of a two-layer cardiac tissue cultured for an additional 3 days after assembly.
Movie S11. Response of Tissue-Velcro (day 5) to epinephrine (300 nM) stimulation.
Reference (*54*)

REFERENCES AND NOTES

1. G. Macchiarelli, O. Ohtani, S. A. Nottola, T. Stallone, A. Camboni, I. M. Prado, P. M. Motta, A micro-anatomical model of the distribution of myocardial endomysial collagen. *Histol. Histopathol.* **17**, 699–706 (2002).
2. P. J. Hanley, A. A. Young, I. J. LeGrice, S. G. Edgar, D. S. Loiselle, 3-Dimensional configuration of perimysial collagen fibres in rat cardiac muscle at resting and extended sarcomere lengths. *J. Physiol.* **517** (Pt. 3), 831–837 (1999).
3. J. W. Holmes, T. K. Borg, J. W. Covell, Structure and mechanics of healing myocardial infarcts. *Annu. Rev. Biomed. Eng.* **7**, 223–253 (2005).
4. P. Camelliti, T. K. Borg, P. Kohl, Structural and functional characterisation of cardiac fibroblasts. *Cardiovasc. Res.* **65**, 40–51 (2005).

5. P. Helm, M. F. Beg, M. I. Miller, R. L. Winslow, Measuring and mapping cardiac fiber and laminar architecture using diffusion tensor MR imaging. *Ann. N. Y. Acad. Sci.* **1047**, 296–307 (2005).
6. M. Montgomery, B. Zhang, M. Radisic, Cardiac tissue vascularization: From angiogenesis to microfluidic blood vessels. *J. Cardiovasc. Pharmacol. Ther.* **19**, 382–393 (2014).
7. M. E. Kolewe, H. Park, C. Gray, X. Ye, R. Langer, L. E. Freed, 3D structural patterns in scalable, elastomeric scaffolds guide engineered tissue architecture. *Adv. Mater.* **25**, 4459–4465 (2013).
8. G. C. Engelmayr Jr., M. Cheng, C. J. Bettinger, J. T. Borenstein, R. Langer, L. E. Freed, Accordion-like honeycombs for tissue engineering of cardiac anisotropy. *Nat. Mater.* **7**, 1003–1010 (2008).
9. M. E. Kolewe, H. Park, C. Gray, X. Ye, R. Langer, L. E. Freed, 3D structural patterns in scalable, elastomeric scaffolds guide engineered tissue architecture. *Adv. Mater.* **25**, 4459–4465 (2013).
10. W. L. Stoppel, D. Hu, I. J. Domian, D. L. Kaplan, L. D. Black III, Anisotropic silk biomaterials containing cardiac extracellular matrix for cardiac tissue engineering. *Biomed. Mater.* **10**, 034105 (2015).
11. S. R. Shin, B. Aghaei-Ghareh-Bolagh, X. Gao, M. Nikkhah, S. M. Jung, A. Dolatshahi-Pirouz, S. B. Kim, S. M. Kim, M. R. Dokmeci, X. S. Tang, A. Khademhosseini, Layer-by-layer assembly of 3D tissue constructs with functionalized graphene. *Adv. Funct. Mater.* **24**, 6136–6144 (2014).
12. N. Thavandiran, N. Dubois, A. Mikryukov, S. Massé, B. Beca, C. A. Simmons, V. S. Deshpande, J. P. McGarry, C. S. Chen, K. Nanthakumar, G. M. Keller, M. Radisic, P. W. Zandstra, Design and formulation of functional pluripotent stem cell-derived cardiac microtissues. *Proc. Natl. Acad. Sci. U.S.A.* **110**, E4698–E4707 (2013).
13. M. Radisic, H. Park, H. Shing, T. Consi, F. J. Schoen, R. Langer, L. E. Freed, G. Vunjak-Novakovic, Functional assembly of engineered myocardium by electrical stimulation of cardiac myocytes cultured on scaffolds. *Proc. Natl. Acad. Sci. U.S.A.* **101**, 18129–18134 (2004).
14. N. K. Paschos, W. E. Brown, R. Eswaramoorthy, J. C. Hu, K. A. Athanasiou, Advances in tissue engineering through stem cell-based co-culture. *J. Tissue Eng. Regen. Med.* **9**, 488–503 (2015).
15. T. Xu, W. Zhao, J.-M. Zhu, M. Z. Albanna, J. J. Yoo, A. Atala, Complex heterogeneous tissue constructs containing multiple cell types prepared by inkjet printing technology. *Biomaterials* **34**, 130–139 (2013).
16. L. Leng, A. McAllister, B. Zhang, M. Radisic, A. Günther, Mosaic hydrogels: One-step formation of multiscale soft materials. *Adv. Mater.* **24**, 3650–3658 (2012).
17. R. Derda, A. Laromaine, A. Mammoto, S. K. Tang, T. Mammoto, D. E. Ingber, G. M. Whitesides, Paper-supported 3D cell culture for tissue-based bioassays. *Proc. Natl. Acad. Sci. U.S.A.* **106**, 18457–18462 (2009).
18. B. Mosadegh, B. E. Dabiri, M. R. Lockett, R. Derda, P. Campbell, K. K. Parker, G. M. Whitesides, Three-dimensional paper-based model for cardiac ischemia. *Adv. Healthc. Mater.* **3**, 1036–1043 (2014).
19. R. T. Tran, P. Thevenot, D. Gyawali, J. C. Chiao, L. Tang, J. Yang, Synthesis and characterization of a biodegradable elastomer featuring a dual crosslinking mechanism. *Soft Matter* **6**, 2449–2461 (2010).
20. C. Mekkaoui, S. Huang, H. H. Chen, G. Dai, T. G. Reese, W. J. Kostis, A. Thiagalingam, P. Maurovich-Horvat, J. N. Ruskin, U. Hoffmann, M. P. Jackowski, D. E. Sosnovik, Fiber architecture in remodeled myocardium revealed with a quantitative diffusion CMR tractography framework and histological validation. *J. Cardiovasc. Magn. Reson.* **14**, 70 (2012).
21. S. S. Nunes, J. W. Miklas, J. Liu, R. Aschar-Sobbi, Y. Xiao, B. Zhang, J. Jiang, S. Massé, M. Gagliardi, A. Hsieh, N. Thavandiran, M. A. Laflamme, K. Nanthakumar, G. J. Gross, P. H. Backx, G. Keller, M. Radisic, Biowire: A platform for maturation of human pluripotent stem cell–derived cardiomyocytes. *Nat. Methods* **10**, 781–787 (2013).
22. V. H. Barocas, R. T. Tranquillo, An anisotropic biphasic theory of tissue-equivalent mechanics: The interplay among cell traction, fibrillar network deformation, fibril alignment, and cell contact guidance. *J. Biomech. Eng.* **119**, 137–145 (1997).
23. W. Bian, N. Badie, H. D. Himel IV, N. Bursac, Robust T-tubulation and maturation of cardiomyocytes using tissue-engineered epicardial mimetics. *Biomaterials* **35**, 3819–3828 (2014).
24. A. M. Blakely, K. L. Manning, A. Tripathi, J. R. Morgan, Bio-pick, place, and perfuse: A new instrument for three-dimensional tissue engineering. *Tissue Eng. Part C Methods* **21**, 737–746 (2015).
25. X. Ye, L. Lu, M. E. Kolewe, K. Hearon, K. M. Fischer, J. Coppeta, L. E. Freed, Scalable units for building cardiac tissue. *Adv. Mater.* **26**, 7202–7208 (2014).
26. S. F. Nagueh, G. Shah, Y. Wu, G. Torre-Amione, N. M. P. King, S. Lahmers, C. C. Witt, K. Becker, S. Labeit, H. L. Granzier, Altered titin expression, myocardial stiffness, and left ventricular function in patients with dilated cardiomyopathy. *Circulation* **110**, 155–162 (2004).
27. S. M. Weis, J. L. Emery, K. D. Becker, D. J. McBride Jr., J. H. Omens, A. D. McCulloch, Myocardial mechanics and collagen structure in the osteogenesis imperfecta murine (*oim*). *Circ. Res.* **87**, 663–669 (2000).
28. C. Coirault, J.-L. Samuel, D. Chemla, J.-C. Pourny, F. Lambert, F. Marotte, Y. Lecarpentier, Increased compliance in diaphragm muscle of the cardiomyopathic Syrian hamster. *J. Appl. Physiol.* **85**, 1762–1769 (1998).
29. J. H. Omens, Stress and strain as regulators of myocardial growth. *Prog. Biophys. Mol. Biol.* **69**, 559–572 (1998).
30. D. A. Narmoneva, R. Vukmirovic, M. E. Davis, R. D. Kamm, R. T. Lee, Endothelial cells promote cardiac myocyte survival and spatial reorganization: Implications for cardiac regeneration. *Circulation* **110**, 962–968 (2004).
31. R. K. Iyer, D. Odedra, L. L. Chiu, G. Vunjak-Novakovic, M. Radisic, Vascular endothelial growth factor secretion by nonmyocytes modulates Connexin-43 levels in cardiac organoids. *Tissue Eng. Part A* **18**, 1771–1783 (2012).
32. B. Korecky, C. M. Hai, K. Rakusan, Functional capillary density in normal and transplanted rat hearts. *Can. J. Physiol. Pharmacol.* **60**, 23–32 (1982).
33. K. Rakusan, B. Korecky, The effect of growth and aging on functional capillary supply of the rat heart. *Growth* **46**, 275–281 (1982).
34. S. Bhatia, U. Balis, M. Yarmush, M. Toner, Effect of cell–cell interactions in preservation of cellular phenotype: Cocultivation of hepatocytes and nonparenchymal cells. *FASEB J.* **13**, 1883–1900 (1999).
35. R. K. Iyer, L. L. Y. Chiu, M. Radisic, Microfabricated poly(ethylene glycol) templates enable rapid screening of triculture conditions for cardiac tissue engineering. *J. Biomed. Mater. Res. A* **89A**, 616–631 (2009).
36. M. D. Chamberlain, R. Gupta, M. V. Sefton, Chimeric vessel tissue engineering driven by endothelialized modules in immunosuppressed Sprague-Dawley rats. *Tissue Eng. Part A* **17**, 151–160 (2011).
37. M. D. Chamberlain, R. Gupta, M. V. Sefton, Bone marrow-derived mesenchymal stromal cells enhance chimeric vessel development driven by endothelial cell-coated microtissues. *Tissue Eng. Part A* **18**, 285–294 (2012).
38. W. Wu, R. A. Allen, Y. Wang, Fast-degrading elastomer enables rapid remodeling of a cell-free synthetic graft into a neoartery. *Nat. Med.* **18**, 1148–1153 (2012).
39. H. Sekine, T. Shimizu, K. Hobo, S. Sekiya, J. Yang, M. Yamato, H. Kurosawa, E. Kobayashi, T. Okano, Endothelial cell coculture within tissue-engineered cardiomyocyte sheets enhances neovascularization and improves cardiac function of ischemic hearts. *Circulation* **118**, S145–S152 (2008).
40. O. Caspi, A. Lesman, Y. Basevitch, A. Gepstein, G. Arbel, I. H. M. Habib, L. Gepstein, S. Levenberg, Tissue engineering of vascularized cardiac muscle from human embryonic stem cells. *Circ. Res.* **100**, 263–272 (2007).
41. K. R. Stevens, K. L. Kreutziger, S. K. Dupras, F. S. Korte, M. Regnier, V. Muskheli, M. B. Nourse, K. Bendixen, H. Reinecke, C. E. Murry, Physiological function and transplantation of scaffold-free and vascularized human cardiac muscle tissue. *Proc. Natl. Acad. Sci. U.S.A.* **106**, 16568–16573 (2009).
42. R. J. Lee, A. Hinson, S. Helgerson, R. Bauernschmitt, H. N. Sabbah, Polymer-based restoration of left ventricular mechanics. *Cell Transplant.* **22**, 529–533 (2013).
43. R. Hashizume, K. L. Fujimoto, Y. Hong, J. Guan, C. Toma, K. Tobita, W. R. Wagner, Biodegradable elastic patch plasty ameliorates left ventricular adverse remodeling after ischemia–reperfusion injury: A preclinical study of a porous polyurethane material in a porcine model. *J. Thorac. Cardiovasc. Surg.* **146**, 391–399.e391 (2013).
44. G. M. Fomovsky, J. R. Macadangdang, G. Ailawadi, J. W. Holmes, Model-based design of mechanical therapies for myocardial infarction. *J. Cardiovasc. Transl. Res.* **4**, 82–91 (2011).
45. G. M. Fomovsky, S. A. Clark, K. M. Parker, G. Ailawadi, J. W. Holmes, Anisotropic reinforcement of acute anteroapical infarcts improves pump function. *Circ. Heart Fail.* **5**, 515–522 (2012).
46. B. Bhana, R. K. Iyer, W. L. Chen, R. Zhao, K. L. Sider, M. Likhitpanichkul, C. A. Simmons, M. Radisic, Influence of substrate stiffness on the phenotype of heart cells. *Biotechnol. Bioeng.* **105**, 1148–1160 (2010).
47. J. Yang, M. Yamato, T. Shimizu, H. Sekine, K. Ohashi, M. Kanzaki, T. Ohki, K. Nishida, T. Okano, Reconstruction of functional tissues with cell sheet engineering. *Biomaterials* **28**, 5033–5043 (2007).
48. B. Zhang, J. V. Green, S. K. Murthy, M. Radisic, Label-free enrichment of functional cardiomyocytes using microfluidic deterministic lateral flow displacement. *PLOS One* **7**, e37619 (2012).
49. M. S. Sacks, C. J. Chuong, Biaxial mechanical properties of passive right ventricular free wall myocardium. *J. Biomech. Eng.* **115**, 202–205 (1993).
50. D. Rappaport, D. Adam, P. Lysyansky, S. Riesner, Assessment of myocardial regional strain and strain rate by tissue tracking in B-mode echocardiograms. *Ultrasound Med. Biol.* **32**, 1181–1192 (2006).
51. C. J. Chuong, M. S. Sacks, G. Templeton, F. Schwiep, R. L. Johnson Jr., Regional deformation and contractile function in canine right ventricular free wall. *Am. J. Physiol.* **260**, H1224–H1235 (1991).
52. R. Rezakhaniha, A. Agianniotis, J. T. C. Schrauwen, A. Griffa, D. Sage, C. V. C. Bouten, F. N. van de Vosse, M. Unser, N. Stergiopulos, Experimental investigation of collagen waviness and orientation in the arterial adventitia using confocal laser scanning microscopy. *Biomech. Model. Mechanobiol.* **11**, 461–473 (2012).

53. J. W. Miklas, S. M. Dallabrida, L. A. Reis, N. Ismail, M. Rupnick, M. Radisic, QHREDGS enhances tube formation, metabolism and survival of endothelial cells in collagen-chitosan hydrogels. *PLOS One* **8**, e72956 (2013).
54. P. Simpson, Stimulation of hypertrophy of cultured neonatal rat heart cells through an α_1-adrenergic receptor and induction of beating through an α_1-and β_1-adrenergic receptor interaction. Evidence for independent regulation of growth and beating. *Circ. Res.* **56**, 884–894 (1985).

Acknowledgments: We thank G. Vunjak-Novakovic for helpful feedback on the manuscript. **Funding:** This work is funded by the Canadian Institutes of Health Research (CIHR) Operating Grant (MOP-126027), Heart and Stoke Foundation GIA T6946, the NSERC Discovery Grant (RGPIN 326982-10), NIH Grant 2R01 HL076485, McLean Fellowship (to M.R.), and Steacie Fellowship (to M.R.). M.M. is supported by NSERC Vanier Graduate Scholarship. **Author contribution:** B.Z. and M.M. envisioned the Tissue-Velcro concept, designed and performed the experiments, analyzed the data, and prepared the manuscript. L.D.-H. performed polymer synthesis, polymer degradation measurement, polymer mechanical testing analysis, LDH assay, and contributed to the editing of the manuscript. A.K. performed polymer mechanical testing. M.R. supervised the work and prepared the manuscript. **Competing interests:** M.R. and B.Z. are cofounders of TARA Biosystems and hold equity in this company.

Submitted 3 April 2015
Accepted 13 July 2015
Published 21 August 2015
10.1126/sciadv.1500423

Citation: B. Zhang, M. Montgomery, L. Davenport-Huyer, A. Korolj, M. Radisic, Platform technology for scalable assembly of instantaneously functional mosaic tissues. *Sci. Adv.* **1**, e1500423 (2015).